



# Experimental Verification of Low-Pressure Kinetics Model for Direct Synthesis of Dimethyl Carbonate Over CeO<sub>2</sub> Catalyst

G. Ibrahim<sup>1,3</sup> · A. Abdelbar<sup>1</sup> · H. A. Choudhury<sup>1</sup> · M. S. Challiwala<sup>1</sup> · A. Prakash<sup>5</sup> · K. Mondal<sup>4</sup> · S. Solim<sup>5</sup> · Nimir O. Elbashir<sup>1,2</sup>

Accepted: 12 August 2024  
© The Author(s) 2024

## Abstract

Dimethyl carbonate (DMC) has emerged as a promising candidate for sustainable chemical processes due to its remarkable versatility and low toxicity. From a green chemistry perspective, the direct synthesis of DMC has been considered the most promising route, as water is the only byproduct generated in the reaction between CO<sub>2</sub> and methanol. However, this synthetic route has faced significant thermodynamic limitations, even at elevated pressure conditions. Therefore, a two-part study explored low-pressure synthesis of DMC via the direct route, and a low-pressure kinetic model for the CeO<sub>2</sub> catalyst was developed based on the results. Proposed Langmuir–Hinshelwood mechanisms were verified using experimental data generated in our labs. The investigation suggests that DMC formation in the direct synthetic route is a surface reaction of CO<sub>2</sub> and methanol on the catalyst. The kinetic model predictions closely aligned with experimental data, demonstrating a 17% mean absolute percentage error and indicating a high level of predictability. Additionally, a rigorous assessment was conducted on CO<sub>2</sub> fixations in DMC synthesis, quantifying CO<sub>2</sub> capture and its conversion into stable or high-value products, formally designated as CO<sub>2</sub> Fixation (CO2Fix). The CO2Fix analysis revealed that, at a conversion rate of 27%, the process can achieve a "net zero" state when operated at an approximate pressure of 30 bar, thereby supporting the viability of low-pressure synthesis. Increasing the conversion rate to levels exceeding 95% significantly enhances the CO2Fix metric, potentially surpassing 3.5 or higher.

**Keywords** CO<sub>2</sub> conversion · Kinetics model · CeO<sub>2</sub>-catalysts · Direct DMC synthesis · CO2Fix · Sustainable processes · Mean absolute percentage error

## 1 Introduction

Dimethyl carbonate (DMC) is a simple organic carbonate molecule with an important role in the chemical industry due to its versatility and broad applications. DMC has been primarily utilized as a solvent, fuel additive, and reactant. Its low toxicity to human health and the environment makes DMC a green solvent and aligns with the principles of green chemistry; therefore, its use promotes sustainability in industrial processes [1]. DMC serves as a substitute for hazardous compounds like ketones or acetate esters in various applications, such as a paint solvent or a solvent in rechargeable lithium batteries.

Before 1980, the exclusive method for producing DMC involved the phosgenation of methanol (MeOH), which utilized highly toxic substances such as phosgene and other corrosive chemicals to recycle phosgene. To eliminate the use of phosgene, other processes for producing DMC have

---

G. Ibrahim and H. A. Choudhury equal contributions by both authors.

✉ Nimir O. Elbashir  
nelbashir@tamu.edu

<sup>1</sup> Chemical Engineering Program, Texas A&M University at Qatar, PO Box 23874, Doha, Qatar

<sup>2</sup> TEES Gas & Fuels Research Centre (GFRC), College Station, TX, USA

<sup>3</sup> Artie McFerrin Department of Chemical Engineering, Texas A&M University, College Station, TX, USA

<sup>4</sup> Shell Technology Center, Bangalore, India

<sup>5</sup> Qatar Shell Technology Research Center, QSTP, Doha, Qatar

been discovered and implemented. EniChem spearheaded the oxidative carbonylation of MeOH by employing a single redox catalyst, CuCl. This method uses MeOH, CO, and O<sub>2</sub> as reactants to produce DMC and water. However, in this reaction, a substantial risk of explosion and toxicity arises from the presence of O<sub>2</sub> and CO. To mitigate this risk, O<sub>2</sub> was replaced with nitrogen oxides [1].

Significant efforts have been directed at overcoming challenges in conventional processes for DMC production, such as MeOH phosgenation and oxy-carbonylation, and methyl nitrite carbonylation. The focus has been on developing alternative routes to mitigate environmental impacts and human health risks. For DMC to qualify as a green solvent, its production process must be environmentally friendly, avoiding toxic and hazardous pathways. Among the various DMC synthesis methods, the direct reaction of CO<sub>2</sub> and MeOH, commonly known as direct synthesis, has emerged as the most attractive pathway. The direct synthesis route aligns with principles of green chemistry and sustainable development as it promotes the consumption of CO<sub>2</sub>, which is non-toxic, nonflammable, noncorrosive, and abundantly available as a point source. Likewise, MeOH exhibits lower toxicity than the chemicals used in alternative routes and is economically appealing due to its cost.

However, direct synthesis of DMC has been thermodynamically unfavorable due to equilibrium limitations [1]. Even under thermodynamically favorable high-pressure conditions (~100 bar), DMC yield has been shown at <1%. Heterogeneous catalysts such as CeO<sub>2</sub> and ZrO<sub>2</sub> have been reported to exhibit higher selectivity toward DMC in the direct synthesis route. These catalyst systems have been shown to produce a DMC yield of ~1%, with a selectivity range of 60–90% [2]. Table 1 details the types of heterogeneous catalysts for the direct synthesis of DMC. CeO<sub>2</sub> remains a popular choice as an active metal, but combined oxides like ZrO<sub>2</sub> and promoters such as La<sub>2</sub>O<sub>3</sub> show higher performance due to optimized acid–base properties that prevent Ce<sup>4+</sup> reduction during the reaction. Other metals, like V<sub>2</sub>O<sub>5</sub> modified with H<sub>3</sub>PO<sub>4</sub> and Cu-Ni/VSO, exhibit higher yields for direct synthesis. This improvement is attributed to the catalysts' ability to activate CO<sub>2</sub> and CH<sub>3</sub>OH at the active sites. Specifically, the direct interaction between V and P in H<sub>3</sub>PO<sub>4</sub>/V<sub>2</sub>O<sub>5</sub> creates effective Brønsted acid sites, enhancing the formation of DMC.

Therefore, an effective method for shifting the equilibrium to achieve high conversion in DMC synthesis from CO<sub>2</sub> and MeOH is essential. Optimal conditions for DMC production can be achieved through innovative approaches such as in-situ water removal using novel water scavengers, parallel reactions that utilize water to generate valuable by-products, or advanced reactors [9]. For instance, a catalytic distillation column, based on reactive distillation (RD) principles, has been shown to not only reduce contact

**Table 1** Heterogeneous catalysts for the direct production of DMC

Catalyst	Operating conditions	DMC yield( $y_{DMC}$ )	Ref
CeO <sub>2</sub>	-, 130 °C	0.8	[3]
ZrO <sub>2</sub>	50 bar, 140–189 °C	0.28	[4]
ZrO <sub>2</sub> catalysts	50 bar, 140–189 °C	0.6	[5]
Ce <sub>0.6</sub> Zr <sub>0.4</sub> O <sub>2</sub>	60 bar, 170 °C	0.6	[6]
Ga <sub>2</sub> O <sub>3</sub> /Ce <sub>0.6</sub> ZrO <sub>2</sub>	60 bar, 170 °C	2.4	[6]
La <sub>2</sub> O <sub>3</sub> /Ce <sub>0.6</sub> ZrO <sub>2</sub>	60 bar, 170 °C	2.25	[6]
Ni <sub>2</sub> O <sub>3</sub> /Ce <sub>0.6</sub> ZrO <sub>2</sub>	60 bar, 170 °C	1.9	[6]
Fe <sub>2</sub> O <sub>3</sub> /Ce <sub>0.6</sub> ZrO <sub>2</sub>	60 bar, 170 °C	1.85	[6]
Y <sub>2</sub> O <sub>3</sub> /Ce <sub>0.6</sub> ZrO <sub>2</sub>	60 bar, 170 °C	1.8	[6]
Al <sub>2</sub> O <sub>3</sub> /Ce <sub>0.6</sub> ZrO <sub>2</sub>	60 bar, 170 °C	1.6	[6]
H <sub>3</sub> PO <sub>4</sub> modified V <sub>2</sub> O <sub>5</sub>	6 bar, 140 °C	9.2	[7]
CeO <sub>2</sub> /ZrO <sub>2</sub>	50 bar, 160 °C	1.76	[5]
Cu-Ni/VSO	9 bar, 180 °C	9	[8]

time but avert DMC hydrolysis by rapidly extracting water, ensuring both efficient reaction conditions and intensified processes. Recent studies by Stoian et al. [9] involved direct DMC synthesis using a lanthanum-promoted CeO<sub>2</sub> catalyst and 2-cyano pyridine (2-CP) as a dehydrating agent. Stoian et al. [9] reported MeOH conversion of >95% and selectivity of >99% per pass continuously at a pressure of 30 bar and a temperature of 120 °C [9, 10]. While the study by Stoian et al. [9] presented a cutting-edge direct DMC synthesis process, the authors encountered several process challenges, particularly regarding 2-CP conversion and recycling. Additionally, 2-CP presents several issues due to its condensation in the reactor tubes/condenser, where there is a temperature gradient. Owing to these facts, the 2-CP combined process does not offer a complete solution for use as an alternative pathway in direct DMC synthesis, and investigations to determine alternative solutions remain underway [11]. Moreover, economic assessment conducted by Choi et al. [11] using 2-CP as a water scavenger showcased an economically unfavorable option due to high regeneration and production cost of 2-CP molecules. This work of Choi et al. [11] clearly hints seeking alternative pathways such RD.

RD is an attractive process route for equilibrium-limited reactions that increase a reactants' conversion by continuously removing the products from the reaction system. An RD is a well-known alternative to conventional processes, especially for equilibrium reactions such as esterification, ester hydrolysis, and etherification [12–18]. RD offers several process advantages such as avoiding azeotropes, shifting the equilibrium towards the product side, reducing side products, providing direct heat integration opportunities, avoiding hot spots, capital saving, lesser operating pressure (10–20 bars), and decreasing catalyst quantity. In the direct synthesis, DMC and MeOH tend to form an azeotrope,

further complicating the synthesis process. Therefore, using an RD for the reaction and separation of DMC could be a significant development in the context of direct synthesis.

Hu et al. [18] studied DMC synthesis with in-situ ethylene oxide using a homogenous RD model with a fixed bed reactor using an equation-based modeling tool gPRPOMS. They observed the equilibrium conversion of MeOH at up to 99.5% in RD setup when operating at 15 bar. Wang et al. [19] studied a non-equilibrium model of the RD process for DMC synthesis over a solid catalyst for urea metanalysis, reporting the effect of pressure and temperature on the DMC yield. An assessment of the effect of pressure on DMC yield within the 1–15 bars range revealed that increased pressure is advantageous for the reaction but introduces a complication for product separation. In their book chapter, Wang et al. [19] reported the synthesis of DMC through catalytic RD using urea and methanol over a solid base catalyst at 9-bars pressure. The authors used a non-equilibrium model to present the column's packing section, and the heterogeneous catalyzed synthesis of DMC in the RD process was treated as pseudo-homogenous. In another study, Huang et al. [20] successfully demonstrated RD-DMC synthesis at 1 bar by transesterifying propylene carbonate using ASPEN Plus® while employing an equilibrium stage model. Cumulatively, these observations imply that reduced operating pressure could be advantageous within the framework of RD for DMC synthesis.

Therefore, developing a kinetic model for low-pressure DMC synthesis becomes imperative to further advance the process and scale it up. Such a model would enable a more comprehensive exploration of the intricate interplay between reaction kinetics, pressure dynamics, and product separation efficiency. In essence, a kinetic model for low-pressure DMC synthesis holds the potential to significantly contribute to the progress of sustainable and efficient DMC production within the RD framework.

The existing literature base of direct DMC synthesis has predominantly concentrated on high-pressure kinetics for 150–200 bars [21–24]. Santos et al. [21] recently reported a Langmuir–Hinshelwood (L–H) type kinetic model for the direct DMC synthesis process of nano-CeO<sub>2</sub> catalyst powder. This kinetic model was developed for a high-pressure (200 bar) synthetic process, and an investigation was conducted on the effect of several parameters—such as temperature, CO<sub>2</sub>-methanol ratio, and pressure—on reaction rates. The activation energy of 106 kJ/mol was reported for their catalyst. In another study, Marin et al. [23] reported a kinetic model for the direct synthesis of DMC on a ceria nanorod catalyst at a slightly low pressure of 137 bar. They reported a much lower activation energy, 65 kJ/mol, than the conventional ceria powder catalyst reported in the past. To address the unique challenges and dynamics associated with low-pressure conditions, it is imperative to leverage the

insights gained from studies on high-pressure kinetics and apply them judiciously. This sets the stage for us to pioneer research aiming to understand the intricacies of low-pressure DMC synthesis and provide a foundation for the development of a kinetic model for a widely used nano-CeO<sub>2</sub>-based catalyst that aligns with the demands of the direct synthetic route. In developing the kinetic model, we aim to investigate the influence of different parameters—such as temperature, catalyst mass, initial CO<sub>2</sub>/MeOH ratio, and pressure—on the reaction rates.

Several theoretical works on RD for DMC synthesis show potential for future applications. However, RD typically operates at relatively low pressures (approximately 10–20 bar), requiring a kinetic model to estimate the product yields for pilot-scale experiments. The existing kinetic models, as reviewed in the manuscript, are designed for higher pressure ranges (>150 bar) and are unsuitable for RD setups. This study aims to develop a kinetic model that predicts DMC yields at lower pressure ranges, which is suitable for simulating the RD process for scale-up studies. Our goal is to create an experimentally validated kinetic model for direct DMC synthesis under low-pressure conditions typical of RD setups.

Furthermore, we investigated the CO<sub>2</sub> footprint analysis of direct DMC synthesis at low pressure and compared its values with high-pressure conditions. This is to set the target to achieve the net-zero state for such a process in-order to optimize it around that state. In a recent publication by our group [25], we introduced a metric named CO2Fix that allows for a straightforward estimation of the CO<sub>2</sub> fixation potential of carbon capture and utilization (CCU) technologies. CO2Fix parameters utilize minimal input parameters, such as reaction pressure, temperature, conversion rate, and heat of reaction. The CO2Fix represents the ratio of CO<sub>2</sub> consumed by a CCU process, which is the CO<sub>2</sub> utilized in the DMC synthesis process in our case, to the CCU produced in the same process.

## 2 Experimental Section

### 2.1 Materials and Methods

MeOH and nano-CeO<sub>2</sub> powder, procured from Sigma Aldrich, and CO<sub>2</sub>, sourced locally from NIGP, Qatar, were employed in the catalyst performance evaluation and kinetic experiments. The reactions were conducted in a 150 mL batch reactor (Parker Benchtop autoclave reactor). To ensure precise control over the reaction conditions, the reactor temperature and pressure were meticulously regulated to within  $\pm 2$  °C and  $\pm 0.5$  bar.

Following a typical experimental procedure, about 200 mg of nano-CeO<sub>2</sub> powder catalyst and MeOH were

carefully loaded into the reactor vessel and subsequently heated to the target reaction temperature. A back-pressure regulator maintained a controlled pressure environment set at the desired condition of 30 bar. Upon reaching the desired reaction temperature 110 °C within the reactor, the vapor pressure of MeOH was measured. The next step was the gradual introduction of CO<sub>2</sub> gas into the reactor vessel until the desired pressure was attained. To facilitate effective mixing and agitation, the impeller in the reactor was set to 25% of its maximum capacity, corresponding to a stirring rate of 150 revolutions per minute (rpm). This choice of stirring intensity was carefully optimized to promote efficient mass transfer and minimize external diffusion limitations during the reaction. The reaction was allowed to proceed for a specific predetermined time, during which the system's progress was continually monitored. To quench the reaction and arrest any further advancement, an ice bath was employed, ensuring a sudden reduction in temperature to halt the reaction kinetics. To collect reaction samples for subsequent analysis, aliquots were extracted from the reaction mixture and, to remove any catalyst particles, meticulously filtered through a 0.2-micron syringe filter. This filtration step prevented further reaction progression, thereby preserving the sampled aliquots in their original state. Subsequently, all collected aliquots were stored in controlled refrigeration conditions, to maintain their integrity and prevent any degradation until further analysis.

As outlined in Fig. 1, the experimental setup and procedure were designed to ensure precise control of reaction parameters and provide a robust platform for evaluating the catalyst's performance. The product samples were analyzed by Agilent gas chromatography (Agilent GC7860) with a Flame Ionization Detector (FID) and capillary column (DB-5; 30 m × 0.2 mm, d<sub>f</sub> 0.25 μm). A specific isothermal program was developed for the sample analysis, where the oven temperature was maintained at a constant 50 °C. This temperature was chosen to ensure optimal conditions for the analysis, allowing for precise and consistent results throughout the testing period. The FID was meticulously calibrated before analyzing the reaction samples using different DMC/MeOH solution concentrations. Subsequently, a robust multi-level calibration curve was constructed to determine the response factor, enabling accurate quantification of the DMC concentration in the product mixture obtained from the reactor runs.

Instrumental analysis allowed for the precise determination of the moles of DMC present in the reaction mixture, forming the basis for calculating the yield according to the following equation [26]:

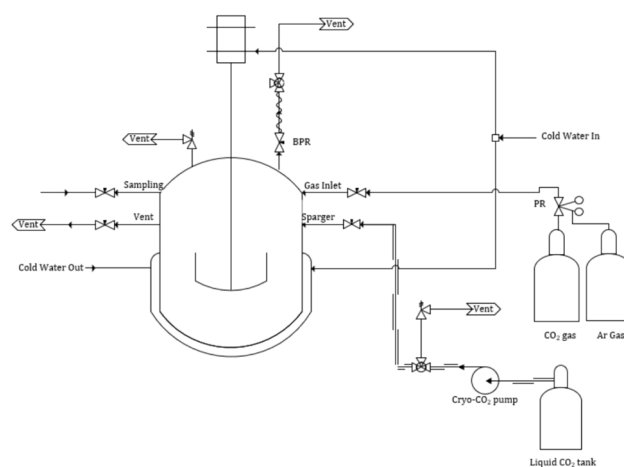


**Fig. 1** The autoclave reactor unit setup comprised a single 130 l vessel mounted to a skeleton body equipped with four main connections to the unit. Each connection had an intended use, which included functions as feed lines and vent lines and performing sample collection. A furnace was clamped around the vessel to supply heat to the unit. Additionally, a water chiller was attached for flange cooling. The rig had one cryopump for feeding liquid CO<sub>2</sub> for critical pressure conditions

$$\begin{aligned}
 y_{DMC} &= \left( \frac{\text{rate}_{DMC\text{Produced}}}{\frac{\text{rate}_{Methanol\text{Consumed}}}{2}} \right) \times 100\% \\
 &= \left( \frac{2 \times \text{rate}_{DMC\text{Produced}}}{\text{rate}_{Methanol\text{Consumed}}} \right) \times 100\% \\
 &= \left( \frac{2 \times \text{moles of DMC produced}}{\text{moles of methanol consumed}} \right) \\
 y_{DMC} &= \frac{2 \times \text{moles of DMC}}{\text{initial moles of methanol}} \times 100\% \quad (1)
 \end{aligned}$$

## 2.2 Characterizations

As a vital introduction to its performance evaluation, the physical properties of the catalyst were meticulously assessed. Two key properties were investigated: the Brunauer–Emmett–Teller (BET) surface area and pore volume. Moreover, crystallographic information was obtained using X-ray diffractometry.

To determine the BET surface area and pore characteristics, nitrogen adsorption–desorption isotherms were measured at a cryogenic temperature of −196.15 °C using a Micromeritics Tri-Star II 3020 instrument. To prepare the sample for analysis, approximately 40 mg of the nano-CeO<sub>2</sub> powder catalyst was carefully heated under an argon flow at 200 °C for 4 h. The surface area was calculated using

the BET equation. Simultaneously, the total pore volume, average pore radius, and pore size distribution were derived by applying the Barrett-Joyner-Halenda method utilizing nitrogen desorption data.

For crystallographic analysis, X-ray diffraction patterns were recorded using a Rigaku Ultima IV diffractometer with Cu ( $K\alpha$ ) radiation at 40 kV and 40 mA. The scans were conducted in the  $2\theta$  range of  $20$ – $110^\circ$  with a step size of  $0.02^\circ$  and a step time of 2 s, ensuring high-resolution data acquisition.

### 3 Results and Discussion

#### 3.1 Catalyst Physical Properties

Figure 2 illustrates the adsorption/desorption isotherms obtained for the nano- $\text{CeO}_2$  powder catalyst under investigation. These isotherms exhibited a distinctive H1-type hysteresis loop, which is characteristic of the mesoporous nature of the material. The H1-type hysteresis loop, classified as a type-IV isotherm, revealed intriguing features. Initially, there was a rapid adsorption uptake at low relative pressures, suggesting the occurrence of capillary condensation within the mesopores. As the relative pressure increased, a pronounced surge in adsorption became evident, emphasizing the mesopores' accessibility to adsorbate molecules.

The analysis of the BET surface area of the nano- $\text{CeO}_2$  powder catalyst revealed a value of  $28 \text{ m}^2/\text{g}$ , highlighting the considerable surface available for potential interactions for direct synthesis of DMC [3]. Concurrently, the Barrett-Joyner-Halenda method enabled the determination of pore

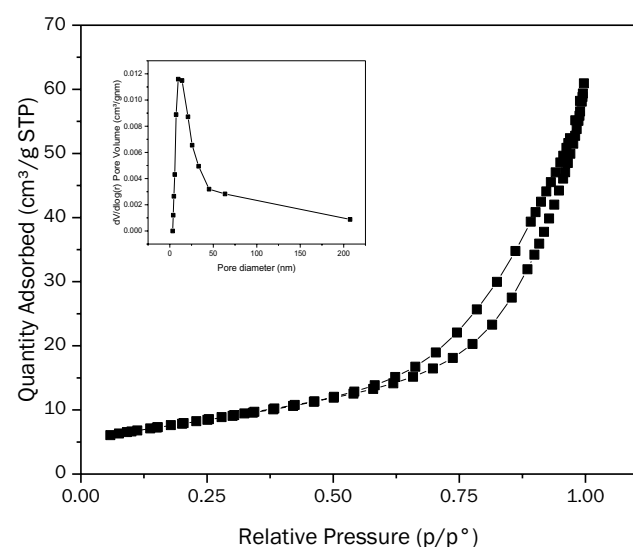


**Fig. 2** BET isotherm of the mesoporous nano- $\text{CeO}_2$  powder catalyst. Inset depicting the average pore diameter of the catalyst

diameters and their distribution. The pore size distribution plots, presented in the inset of Fig. 2, vividly portray a significant volume of pores with diameters below 50 nm. This observation aligns with the calculated average pore volume of 25 nm, providing further evidence of mesopores' consistent and substantial presence throughout the material's structure.

X-ray diffraction analysis was used as a precise tool to investigate the detailed crystalline arrangement of nano- $\text{CeO}_2$  powder catalysts. Figure 3 displays the complex patterns obtained from the X-ray diffraction of the nano- $\text{CeO}_2$  powder catalyst. Upon careful examination, a distinct pattern emerged: the nanoparticles possess a unique crystalline structure, resembling a face-centered cubic arrangement. The measured cell parameter of 0.5411 nm and the associated crystallographic space group  $Fm\bar{3}m$  provide intriguing confirmation, aligning well with the recognized reference JCPDS Card No: 43-1002. These peaks, precisely identified at  $2\theta$  values of  $28.52^\circ$ ,  $33.16^\circ$ ,  $47.59^\circ$ , and  $56.208^\circ$ , were unambiguously attributed to reflection planes (111), (200), (220), and (311), respectively, within the crystalline lattice of the face-centered cubic  $\text{CeO}_2$  structure [27].

#### 3.2 Catalyst Performance in Batch Reactor

To explore the activity and selectivity of the nano- $\text{CeO}_2$  powder catalyst and estimate the equilibrium conversion, a series of preliminary experiments were conducted over varying time intervals, from 1 to 4 h. These experiments aimed to assess the progression of MeOH conversion and DMC yield over time, providing crucial insights into the reaction dynamics. The data obtained from these preliminary experiments revealed that MeOH conversion and DMC yield reached a plateau after 2 h, as evidenced by the results in Fig. 4. This observation suggests that the reaction system

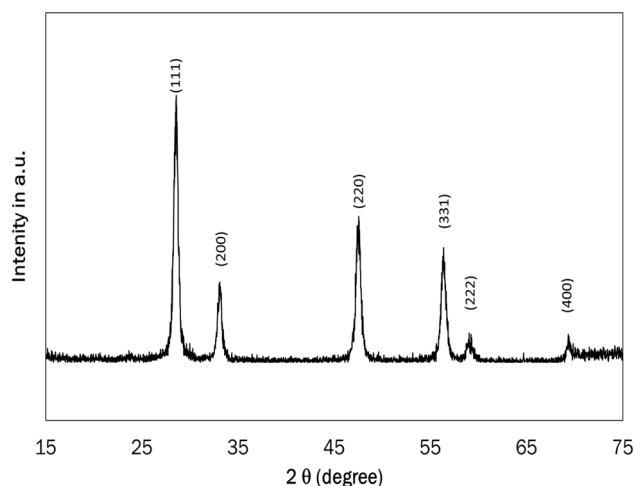


**Fig. 3** X-ray diffraction data of the fresh nano- $\text{CeO}_2$  catalyst



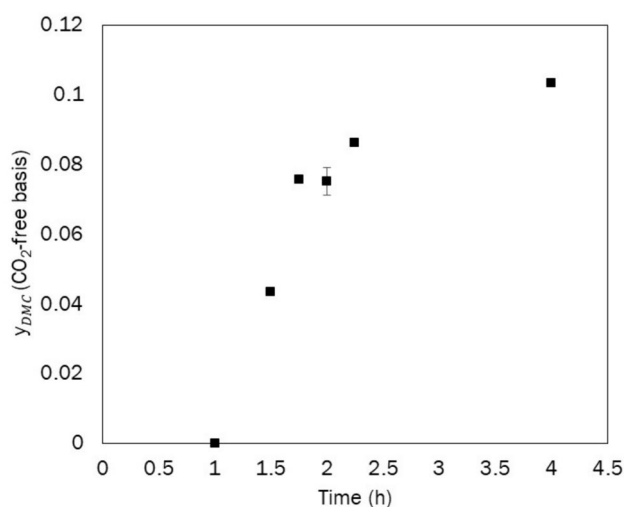


**Fig. 4** Effect of reaction time on the  $y_{DMC}$  (CO<sub>2</sub>-free basis). Cat. mass: 200 mg, total pressure: 30 bar, and MeOH: CO<sub>2</sub>=2 (molar)

attains equilibrium within this timeframe, indicating that further reaction progress is limited beyond this point. Therefore, based on these findings, all subsequent kinetic experiments were standardized to a reaction time of 2 h. It should be noted that the experiment data at 1.75 h is slightly higher than that of the 2 h data point. This could be possibly due to sampling inconsistencies or potential inaccuracies in the GC analysis that could be caused by very low concentration of the DMC near the detection limits of the GC. Further, it should be noted that these samples are from different experiments conducted at different times.

Equilibrium conversion plays a vital role in understanding the reaction's thermodynamic behavior and provides valuable information on the attainable yields under specific conditions. Following recognition of the equilibrium state at  $\geq 2$  h, kinetic analysis of the reaction was focused during this period, enabling a more comprehensive understanding of the catalytic behavior and reaction mechanisms. Rigorous analysis of these kinetic data allowed for deeper insights into the catalyst's performance, the reaction pathways, and any potential rate-limiting steps involved in directly synthesizing DMC from MeOH and CO<sub>2</sub> using the nano-CeO<sub>2</sub> powder catalyst.

### 3.3 Kinetics Experiments and Optimization

#### 3.3.1 Effect of Catalyst Loading

Our study investigated the activity of different catalyst loadings in synthesizing DMC from MeOH and CO<sub>2</sub>. Finding an efficient and selective catalyst for this reaction is paramount to enhancing the process' economic viability and minimizing its environmental impact. The

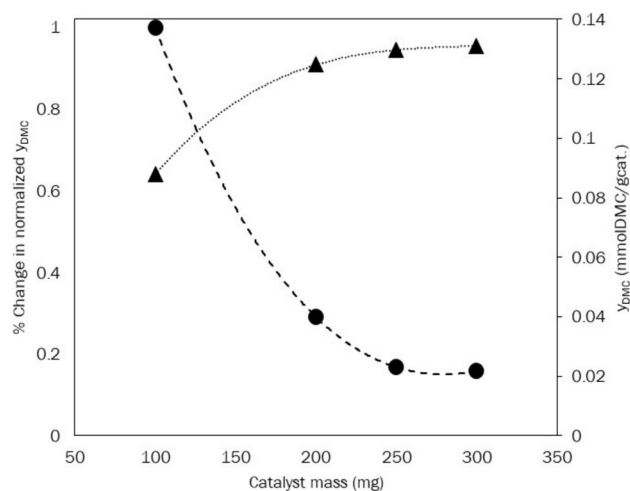


**Fig. 5** Effect of cat. mass on  $y_{DMC}$  (CO<sub>2</sub> free basis). Total pressure: 30 bar. MeOH: CO<sub>2</sub>=2 (molar)

present study selected approximately 100 mg, 200 mg, and 300 mg of catalyst loadings per batch. These catalyst masses were chosen based on previous literature and initial optimization studies to ensure a range of loading conditions. The blank experiment, without any catalyst, served as a reference to understand the inherent thermodynamics of the reaction in the absence of catalysis. To conduct the experiments, a constant temperature of 110 °C was maintained, as this temperature was favorable for the direct synthesis of DMC from MeOH and CO<sub>2</sub>, thereby providing a balance between reaction rates and thermodynamic feasibility.

Moreover, a molar ratio 2:1 (MeOH:CO<sub>2</sub>) was selected to maintain an appropriate stoichiometry for the reaction. During the reaction, aliquots were collected hourly to monitor the  $y_{DMC}$ . A rapid quenching method, placing the reaction mixture in an ice bath, was employed to avoid any disturbance in the equilibrium during sampling. This technique effectively halted the reaction progress and allowed for accurate analysis of the reaction state at each time point. The subsequent filtration of the liquid samples from the catalyst was crucial to arrest the catalytic activity, ensuring that the measured  $y_{DMC}$  were solely attributed to the catalyst's influence and not to continued catalysis during analysis. The results, depicted in Fig. 5, clearly demonstrated the influence of catalyst mass on the reaction kinetics.

Notably, the blank experiment showed no detectable DMC, indicating that there are significant thermodynamic barriers in the direct synthesis of DMC from MeOH and CO<sub>2</sub>, which underscores the importance of catalysis for promoting this transformation [28]. The comparison of different catalyst masses revealed an interesting trend: while the reaction rates increased with an increase in catalyst mass from 100 to 200 mg, further increasing the mass to 300 mg did

not significantly improve the  $y_{DMC}$ . This finding indicates an optimum catalyst mass range (200–300 mg per batch), beyond which an additional catalyst does not significantly enhance the reaction kinetics.

### 3.3.2 Effect of Total Pressure

To evaluate the influence of total pressure on the direct synthesis of DMC from MeOH and CO<sub>2</sub>, the investigation was conducted using carefully controlled experimental conditions. The experimental setup, characterized by an optimal catalyst loading of 200 mg per batch, a temperature of 110 °C, and a molar ratio of 2:1 (MeOH: CO<sub>2</sub>), was consistently maintained throughout the study. The analysis incorporated three distinct reaction pressures: 10, 20, and 27.5 bar, which were chosen to incorporate a broad pressure spectrum and to discern the pressure-dependent behavior of the reaction. The impact of pressure on  $y_{DMC}$  is depicted in Fig. 6. Notably, the results reveal a clear ascending trend in  $y_{DMC}$  as the pressure increases from 10 bar to 27.5 bar. This tendency towards enhanced  $y_{DMC}$  with escalating pressure corresponds to the reaction system's progression towards equilibrium. These findings highlight the pivotal role of pressure as a critical parameter in the direct synthesis of DMC from MeOH and CO<sub>2</sub>, offering valuable insights for process optimization and design.

It is important to note that the observed trend of increasing  $y_{DMC}$  with rising pressure reaches a point of diminishing yields beyond a certain pressure threshold. The analysis of the data indicates that pressures beyond 27.5 bar results in only subtle changes in  $y_{DMC}$ , with the reaction system approaching equilibrium. This phenomenon is consistent with earlier findings reported in the literature [21]. The

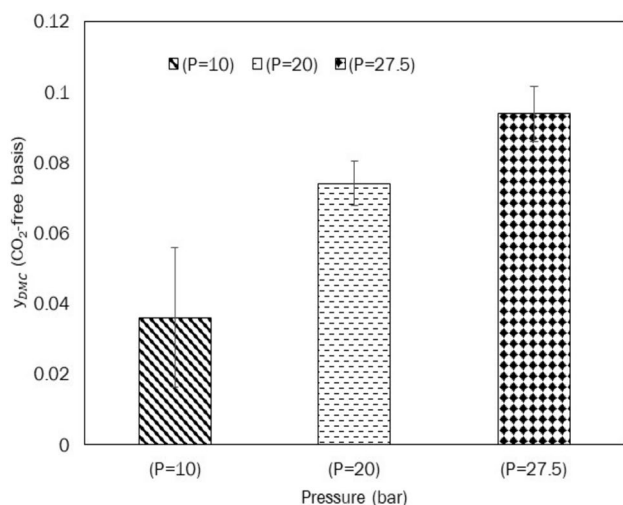


**Fig. 6** Effect of total pressure on  $y_{DMC}$  (CO<sub>2</sub>-free basis). Cat. mass: 200 mg, temperature: 110 °C, and MeOH: CO<sub>2</sub> = 2 (molar)

incremental impact of pressure beyond this threshold necessitates more sophisticated approaches, such as implementing methods to shift the equilibrium to achieve further improvements in  $y_{DMC}$ .

### 3.3.3 Effect of Reaction Temperature

The impact of reaction temperature on the direct synthesis of DMC from MeOH and CO<sub>2</sub> was investigated in a study conducted under controlled conditions. In the control experiment, the reaction temperature was maintained at 30 °C, while all other parameters, including catalyst mass, total pressure, batch time, and impeller speed, were kept constant. The same experimental setup was maintained throughout the investigation, with an optimal catalyst loading of 200 mg/batch, a total pressure of 30 bar, and a molar ratio of 2:1 (MeOH:CO<sub>2</sub>). Three specific reaction temperatures—90, 110, and 120 °C—were chosen to thoroughly examine the temperature dependency of the reaction, enabling precise monitoring of the kinetic regime. The optimal catalyst loading and reactant molar ratio selection were based on prior optimization studies and initial experimental results. The 200 mg/batch catalyst loading yielded the most efficient  $y_{DMC}$  within the earlier identified optimal range of 200–300 mg/batch. Additionally, the molar ratio of 2:1 (MeOH: CO<sub>2</sub>) ensured the appropriate stoichiometry to favor the formation of DMC without excessive reactant consumption. The results of the temperature-dependent experiments are presented in Fig. 7.

As observed, the  $y_{DMC}$  exhibited a notable trend with respect to temperature variations. At the lowest temperature, 90 °C, the yields were relatively moderate. As the temperature was elevated to 110 °C, the  $y_{DMC}$  gradually

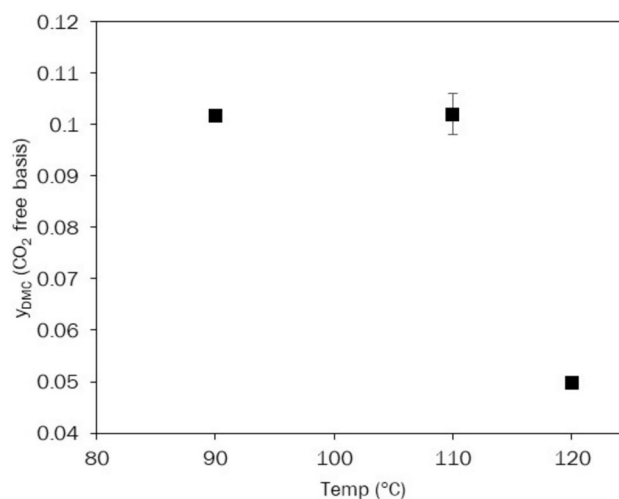


**Fig. 7** Effect of temperature on  $y_{DMC}$  (CO<sub>2</sub> free basis). Cat. mass: 200 mg, total pressure: 30 bar, and MeOH: CO<sub>2</sub> = 2 (molar)

**Table 2** Effect of external mass transfer on  $y_{DMC}$ (CO<sub>2</sub> free basis)

Catalyst mass (mg)	Time (h)	RPM	$y_{DMC}$
200	2	150	0.10
200	2	300	0.11
200	2	600	0.10

**Table 3** Effect of internal mass transfer on  $y_{DMC}$ (CO<sub>2</sub> free basis)

Catalyst mass (mg)	Time (h)	Particle		$y_{DMC}$
		(mesh)	(micron)	
200	2	50–150	297–89	0.07
200	2	> 150	< 89	0.11

increased. The most intriguing finding was that the reaction rates reached their highest point at 110 °C, indicating the optimum temperature for this direct synthesis process. At 120 °C, the  $y_{DMC}$  exhibited a reduction of 50%. This phenomenon may be attributed to the slightly exothermic nature of the reaction at higher temperatures, which results in a decrease in reaction efficiency. At elevated temperatures, the system's thermal energy might promote side reactions or alter the reaction pathway, thereby contributing to decreased  $y_{DMC}$ . Moreover, the complex interplay of various factors, including thermodynamics, kinetics, and diffusion limitations, can influence the reaction rates in different temperature regimes. The rate-determining step might shift at higher temperatures, impacting the overall reaction kinetics and reducing conversion efficiency.

### 3.3.4 Elimination of Internal and External Mass Transfer Diffusion Limitation

To mitigate the influence of external mass transfer limitations, deliberate efforts were undertaken to enhance the catalyst's contact with the bulk media. This was achieved through experimentation involving variations in the impeller speed within the reactor while maintaining the optimal catalyst loading. Specifically, the kinetic experiments systematically employed impeller speeds of 150, 300, and 600 rpm. Table 2 presents the  $y_{DMC}$  obtained at these different stirring rates. The experimental data demonstrates that the  $y_{DMC}$  reaches a saturation point irrespective of the impeller speed, suggesting that external mass transfer limitation does not impact the reaction.

To assess the impact of internal mass transfer limitations on the catalytic direct DMC synthesis. As catalyst particle size is a critical factor influencing the internal diffusion process, different catalyst particle sizes were tested. By segregating the catalyst into two sizes (50–150 mesh and >150 mesh), we aimed to discern potential correlations between

particle size and reaction rates. We focused our investigation on two specific catalyst particle sizes, which were obtained from Sigma Aldrich and used as is. Table 3 presents the  $y_{DMC}$  for the two catalyst particle sizes, showing a slight difference in  $y_{DMC}$  and thus indicating the presence of internal mass transfer diffusion limitations within the catalyst particles. The implications of these findings can be attributed to the characteristics of the CeO<sub>2</sub> catalyst. According to the supplier's specifications, the crystallite size of the CeO<sub>2</sub> is approximately 50 nm, while the BET surface area measured 28 m<sup>2</sup>/g, revealing a type-IV adoption isotherm with a mesoporous structure. Theoretically, the presence of a network of pores within the catalyst particles, as demonstrated by the hysteresis loop in the isotherm, might suggest the possibility of internal diffusion constraints. Based on this study, our kinetic experiments were conducted with catalyst particles of size >150 mesh.

## 3.4 Kinetic Model and Equilibrium Constant

### 3.4.1 Equilibrium Constant

The equilibrium constant is a fundamental concept in chemical thermodynamics, playing a crucial role in understanding the state of chemical reactions at equilibrium [29]. Equilibrium constant is expressed based on the fugacity or activity of the reactants and products. Fugacity, representing the escaping tendency of a substance from its current phase, and activity, reflecting the effective concentration in non-ideal solutions, provide essential insights into the behavior of chemical species in diverse conditions such as high pressures, low temperatures, or concentrated solutions. By accounting for deviations from ideal behavior, the equilibrium constant, involving fugacity or activity constants, offers a more refined and precise depiction of the equilibrium position. Santos et al. [21] estimated the equilibrium constant for DMC synthesis from MeOH and CO<sub>2</sub> using both ideal and real gas models. Their findings indicated that the ideal gas model provided a more accurate estimation of the equilibrium compared to the real gas model. However, the direct synthesis of DMC at lower pressure has been shown to be significantly influenced by liquid–vapor equilibrium, and assuming an ideal gas may introduce some inaccuracies. Despite this consideration, for the sake of simplicity, an ideal gas model was utilized in this work, assuming unity for the fugacity term in the calculations.

The Gibbs Free Energy minimization method was employed for the initial assessment of reaction equilibrium, and the results are depicted in Fig. 8. This figure illustrates the maximum attainable thermodynamic equilibrium  $y_{DMC}$  under normal reaction conditions, spanning temperatures from 50 to 200 °C and pressures ranging between 5 and 100 bars.



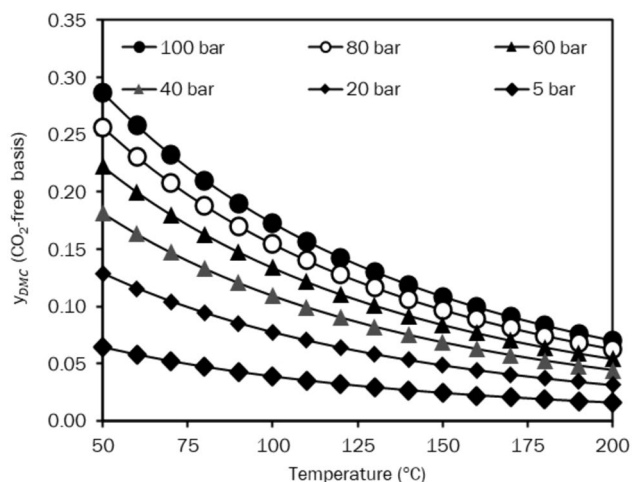


**Fig. 8** A plot of thermodynamic  $y_{DMC}(\text{CO}_2$  free basis) as a function of temperature and pressure in the range of 50–200 °C and 5–100 bars, respectively. The plot presents thermodynamic targets at various operating conditions and at stoichiometric feed

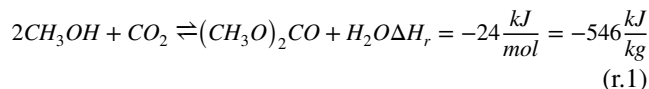
As shown in Fig. 8, even under relatively high temperature and pressure conditions that could yield supercritical phase conditions, the conversion toward DMC remained below 1%. Corroborating with the previous literature [2], these results imply the need for process modification and/or reaction modification, which would result in higher conversions towards DMC. Notably, the low conversion towards DMC is due to the “equilibrium lock” created by the equivalent production of water as a by-product in the reaction. Therefore, process modification—such as the RD in which water may be continuously removed or using a dehydrating agent for in-situ water removal—would result in an equilibrium push toward DMC as the desirable product.

**Table 4** Reaction mechanism for direct synthesis of DMC [21]

Step no	Step description	Reaction	
Step 1	The adsorption of $\text{CO}_2$	$\text{CO}_2 + * \xrightleftharpoons[k_{b1}]{k_{f1}} \text{CO}_2^*$	(r.2)
Step 2	The adsorption of MeOH	$M + * \xrightleftharpoons[k_{b2}]{k_{f2}} M^*$	(r.3)
Step 3	The surface reaction between adsorbed MeOH and $\text{CO}_2$	$\text{CO}_2^* + 2M^* \xrightleftharpoons[k_{b3}]{k_{f3}} \text{DMC}^* + \text{H}_2\text{O}^* + *$	(r.4)
Step 4	The desorption of DMC	$\text{DMC}^* \xrightleftharpoons[k_{b3}]{k_{f4}} \text{DMC} + *$	(r.5)
Step 5	The desorption of $\text{H}_2\text{O}$	$\text{H}_2\text{O}^* \xrightleftharpoons[k_{b5}]{k_{f5}} \text{H}_2\text{O} + *$	(r.6)

### 3.4.2 Kinetic Model

The catalytic direct synthesis of DMC can be expressed as follows:



The direct synthesis of DMC via the L–H mechanism entails the catalytic transformation of MeOH and  $\text{CO}_2$ . The L–H mechanism proposes that the reaction rate depends on the reactants’ adsorption on the catalyst’s surface and their subsequent interactions at the active sites [22, 23]. The competitive adsorption between MeOH and  $\text{CO}_2$  adds complexity to the kinetics, distinguishing it from simple single-step reactions.

In the catalytic direct synthesis of DMC, three stepwise reactions occur. (i) adsorption: the first step involves the adsorption of MeOH and  $\text{CO}_2$  molecules onto the active sites of the catalyst surface. During this stage, the reactants interact with the catalyst’s active sites, forming adsorbed species. (ii) surface reactions: Once adsorbed, the activated methoxy compound and the surface-bound  $\text{CO}_2$  species undergo surface reactions on the catalyst. This surface reaction step involves the transformation of the adsorbed species into intermediate species, such as surface methoxy-carbonate complexes. (iii) desorption: Following the surface reactions, the resulting DMC and water molecules desorb from the catalyst surface into the bulk reaction media. This desorption step completes the primary reactions and allows the liberated DMC and water to diffuse away from the catalyst surface. Each step is considered an elementary reaction, with one notable distinction being the substitution of species concentrations with their corresponding partial pressures.

For the direct synthesis of DMC from CO<sub>2</sub> over the CeO<sub>2</sub> catalyst, the surface reaction has been reported in the literature to be the rate-limiting step [21, 23, 24].

The reaction mechanism, based on the L–H model for DMC production, is shown in Table 4.

By taking  $k_{f3}$  as a common factor:

$$-r_{SR} = k_{f3}([CO_2 *][M *]^2 - \frac{k_{b3}[DMC *][H_2O *][*]}{k_{f3}}) \quad (3)$$

by substituting  $\frac{k_{b3}}{k_{f3}}$  with  $\frac{1}{K_C}$ .

$$-r_{SR} = k_{f3}([CO_2 *][M *]^2 - \frac{[DMC *][H_2O *][*]}{K_C}) \quad (4)$$

where  $K_C$  is the surface reaction equilibrium constant.

As it is not possible to quantify the surface concentrations [\*] experimentally, they were expressed in terms of measurable quantities, where the rate expression assumed the following form:

$$-r_{SR} = \frac{k(P_{CO_2}P_M^2 - \frac{P_D P_H}{K_{eq}})}{(1 + K_{1ads}P_{CO_2} + K_{2ads}P_M + K_{4des}P_D + K_{5des}P_H)^3} \quad (5)$$

Details of the derivation of rate expressions are provided in the supplementary document. The rate expression was rewritten as a function of DMC concentration as only the concentration of DMC was measured from the result of the experiment. Additionally, the rate constant ( $k$ ) was expanded to its full form to include the activation energy ( $E_a$ ) and activation volume ( $\#V$ ), as seen in the following equation:

$$-r_{SR} = \frac{ke^{\frac{-E_a - \#V(P-P_0)}{RdT}} \left( \left(1 - \frac{P_D}{P_{CO_2}}\right)^3 - \frac{P_D^2}{K_{eq}} \right)}{\left(1 + K_{1ads} * P_M * \left(1 - \frac{P_D}{P_{CO_2}}\right) + K_{2ads} * P_{CO_2} * \left(1 - \frac{P_D}{P_{CO_2}}\right)\right)^3} \quad (6)$$

To account for the effect of pressure ( $P$ ), a reference pressure ( $P_0$ ) with a known kinetics constant was required. This information was taken from previously published work on high-pressure direct synthesis of DMC kinetics by Santos et al. [21]. The adsorption terms for DMC and MeOH were neglected for parameter optimization in this study as both materials exist in very low concentrations and were not expected to influence the adsorption term significantly. The activation energy and the adsorption equilibrium constants were obtained from literature (Santos et al. [21]) and substituted in the model. Activation energy is not typically a function of pressure, but it is a function of the catalyst systems. The activation energy for the ceria catalyst, as reported in the study by Santos et al. [21], aligns with findings from other research on ceria catalysts in the direct synthesis of DMC [22, 23]. Consequently, we have adopted this value in

our study. The remaining kinetic parameters to be estimated were  $k$ ,  $K_{eq}$ , and  $\#V$ .

In this paper, the focus was on the development of a kinetic model for a low-pressure system. The surface reaction step was initially considered as the rate-limiting step. However, the possibility of the adsorption and desorption steps functioning as rate-limiting was also investigated. The supplementary document provides a comprehensive derivation of the alternative scenarios conducted to examine this aspect in detail.

**3.4.2.1 Parameter Optimization** The kinetics parameters were adjusted using the low-pressure (10–30 bars) experimental data through minimization of the mean absolute percent error (MAPE) between the estimated DMC mole fraction ( $x_{mi}$ ) obtained from the kinetic model and the DMC mole fraction obtained experimentally ( $x_{ei}$ ).

$$MAPE = \frac{1}{n} \sum_i \left| \frac{x_{ei} - x_{mi}}{x_{ei}} \right| \times 100 \quad (7)$$

where  $x_{mi}$  is the model-predicted DMC mole fraction on a CO<sub>2</sub>-free basis and  $x_{ei}$  is the experimental DMC mole fraction on a CO<sub>2</sub>-free basis.

To assess the mole fraction of DMC on a CO<sub>2</sub>-free basis, the fundamental principles of Dalton's law and the assumption of an ideal gas mixture were employed. The mole fraction of DMC (denoted as  $x_i$ ) was derived from the following relation:

$$x_i = \frac{2 * P_D}{P_M} \quad (8)$$

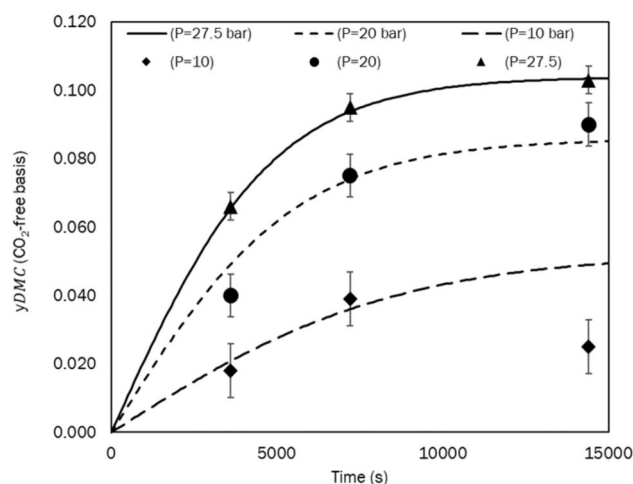


**Fig. 9** Surface reaction dynamics: the model-fitted and experimentally measured DMC concentrations over time in three distinct pressure conditions (10, 20, and 27.5 bar)

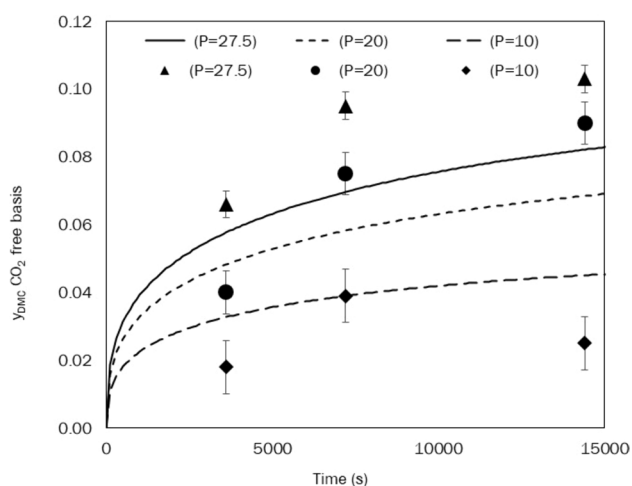


**Fig. 10** CO<sub>2</sub> adsorption reaction dynamics: a comparative study of model-fitted and experimentally measured DMC concentrations over time in three distinct pressure conditions (10, 20, and 27.5 bar)

**Table 5** Optimized kinetics parameters via low-pressure experimental data: MAPE between estimated and experimental DMC mole fractions

Kinetics parameters	Adjusted value
$K$	$1.1510^{-3}$
$\#V$	$-3.776 \times 10^{-4}$
$K_{eq}$	$11.5 \times 10^{-14}$
$K_{1ads}$	$1.0 \times 10^{-6}$
$K_{2ads}$	$1.1 \times 10^{-7}$

where  $P_D$  is the partial pressure of the DMC and  $P_M$  is the initial partial pressure of the MeOH.

The ordinary differential equation (ODE), represented by Eq. 6 (surface reaction rate equation), and the adsorption and desorption rate equation outlined in the supplementary document were solved in R Studio using the direct factorization methods for linear systems, the “dsolve” package, which applies the Livermore Solver for Ordinary Differential Equation, “lsoda,” to integrate the ODE function [30, 31]. Utilizing the Broyden–Fletcher–Goldfarb–Shanno method, the solver function was then nested in an optimization function based on the “optim” package, which is a quasi-Newtonian optimization method. The optim function was set to minimize the MAPE

**Table 6** Tabular representation of the kinetics prediction and comparison with experimental data at temperatures of 90 °C, 110 °C, and 120 °C. The pressure was at 30 bar in all conditions

Kinetics model, CSTR	$y_{DMC}(\text{CO}_2 \text{ free basis}),$ kinetic, (liquid phase)	$y_{DMC}(\text{CO}_2 \text{ free basis}),$ exp., (liquid phase)	% Diff (liquid kinetics. vs. liquid exp.)
90 °C; 30 bar	0.0473	0.102	−115.26
110 °C; 30 bar	0.0611	0.103	−68.47
120 °C; 30 bar	0.0599	0.048	19.90

between experimental and model DMC concentrations, as described in Eq. 7. The optimized kinetic parameters provided a reasonable estimate for DMC concentrations in the ranges studied in this work, with a MAPE of 17% for kinetics models and the surface reaction functioning as the rate-limiting step. Figure 9 shows the model and experimental DMC concentrations over time in three different pressure conditions, drawn from experimental data and the developed surface-reaction-limited kinetics model.

For the adsorption reaction, the studied DMC concentrations within the investigated ranges exhibited a MAPE of 30%, as depicted in Fig. 10. A higher MAPE value of 30% indicated that a mechanism based on the surface reaction as the limiting step is more likely than the reaction being limited by the adsorption of CO<sub>2</sub>.

The experiments described in this section were undertaken to establish a suitable kinetic model that adequately describes the desorption kinetics under study.

Notably, the presentation of fitting data and direct comparison for the desorption reaction was intentionally omitted to concentrate on the fundamental aspects of the investigation. By quantitatively analyzing the MAPE values between the surface reaction and CO<sub>2</sub> adsorption-reaction, it becomes evident that the direct DMC synthesis predominantly adheres to reaction kinetics, with surface reactions as the rate-limiting step. Consequently, kinetic parameters specifically pertaining to the surface reaction were rigorously estimated, and the resultant values are elucidated in Table 5.

**3.4.2.2 Kinetics Validation with Experimental Data** Utilizing the regressed kinetics parameters in Sect. 3.4.2.1, the kinetics model in equation Eq. 5 was implemented in a CSTR model in ASPEN Plus V 14 [30]. The CSTR model closely mirrors the reaction system utilized in this study, discussed in Sect. 2. The CSTR model was configured using an Langmuir–Hinshelwood–Hougen–Watson (LHHW)-type kinetics reaction programmed separately in ASPEN kinetics. In our LHHW modeling, we used a continuous stirred-tank reactor (CSTR) with a total catalyst weight of 200 mg, consistent with our experimental setup, and maintained a reactor volume of 100 mL. The kinetics run was conducted in the same experimental conditions as depicted in Fig. 4, and the results were obtained both in the vapor phase and liquid phase. The Soave–Redlich–Kwong fluid package was

**Table 7** Comparison between thermodynamics and kinetics results

Condition	Thermo yield, CO <sub>2</sub> free basis	$y_{DMC}$ (CO <sub>2</sub> free basis), kinetic, (liquid phase)	$y_{DMC}$ (CO <sub>2</sub> free basis), kinetic, (vapor phase)	Overall kinetics	% Diff (thermo vs. overall kinetics)	% Diff (thermo vs. kinetics vapor phase)
90 °C; 30 bar	0.0977	0.0473	0.0551	0.0547	78.491	77.424
110 °C; 30 bar	0.0791	0.0611	0.0714	0.0704	12.350	10.779
120 °C; 30 bar	0.0733	0.0599	0.0699	0.0685	7.043	4.814

used because the literature has found it has an accurate predictability for the DMC reaction system [32]. The kinetics model developed in this work was tailored for low-pressure conditions that are predominantly gas phase; therefore, the predictability of the model will be superior in gas phase conditions. Nevertheless, the model predicts fairly in liquid phase conditions, specifically, in low-liquid high-vapor fraction conditions. As only the liquid sample was analyzed from the experimental results in the CSTR model, the comparison presented in Table 6 is between the liquid phase prediction from kinetics and the experimental liquid phase results only.

At a low temperature of 90 °C and a pressure of 30 bar, the model prediction deviated significantly from the experimental data by −115%, due to the high liquid and low vapor phases. The error narrowed as the temperature increased and the phase split shifted more towards the vapor phase. This was also observed in comparing the thermodynamics and kinetics results shown in Table 7. As depicted, the highest deviation was at 90 °C, which was the high-liquid, low-vapor condition. Remarkably, the deviation between the thermodynamics and kinetics prediction at 120 °C was below 5%, suggesting the model's efficacy in predicting vapor phase conditions.

The condition of low pressure and high temperature is favorable for the vapor phase. Therefore, the developed kinetics model is expected to provide the highest accuracy in predicting  $y_{DMC}$  in this condition. As the low-pressure, high-temperature condition corresponds to the vapor phase (or higher vapor fraction) and considering that the developed kinetics model achieves reasonable accuracy under these conditions, the developed kinetic model can be confidently used for estimating  $y_{DMC}$  in vapor phase scenarios. However, for liquid phase conditions, the high-pressure model proposed by Santos et al. [21] is more appropriate. Although our current kinetics model employs a mechanism similar to that described in Santos et al. [21], the kinetic parameters in our model are specifically tailored to fit experimental data obtained under low-pressure conditions.

## 4 CO<sub>2</sub> Footprint Analysis

Calculating the CO<sub>2</sub> footprint for chemical processes, especially the direct DMC synthesis process, serves several important purposes. Firstly, such a calculation allows for quantification of the environmental impact of the process, thereby providing valuable insights into its sustainability. By understanding the amount of CO<sub>2</sub> emitted or utilized during DMC synthesis, an assessment of its contribution to climate change and identification of opportunities for improvement are possible.

Secondly, CO<sub>2</sub> footprint calculation is crucial in evaluation of the efficiency of the direct DMC synthesis process. Footprint calculation helps determine the extent to which CO<sub>2</sub> is effectively utilized as a feedstock, thereby optimizing resource utilization and minimizing waste. This information is invaluable for enhancing process efficiency and reducing overall environmental impact.

By quantifying the CO<sub>2</sub> emissions associated with direct DMC synthesis, environmental performance comparisons can be made with other synthesis routes, and opportunities for innovation and improvement can be identified. Further, CO<sub>2</sub> footprint assessment broadens the scope of CCU initiatives. Therefore, through the assessment of the CO<sub>2</sub> footprint of the direct DMC synthesis process, a pathway is paved for integration of CCU strategies aimed at achieving both environmental and economic sustainability. For a CCU process to achieve net CO<sub>2</sub> fixation, the CO<sub>2</sub>Fix must be > 1. The model for the CO<sub>2</sub>Fix contains several parameters that are based on process design considerations, such as the extent of heat integration, unit efficiencies, and choice of cooling technologies for exothermic reactions [25]. By assuming no heat integration and ideal unit efficiencies, the CO<sub>2</sub>Fix can be calculated using the following equation:

$$CO_2Fix = \frac{x_{CO_2} * X_{CO_2}}{Q * \theta + W * \theta} \quad (9)$$

where  $x_{CO_2}$  is the mass fraction of the CO<sub>2</sub> in the feed stream [kg CO<sub>2</sub>/kg feed]. It should be noted that the  $y_{DMC}$  discussed in the previous sections is equal to CO<sub>2</sub> conversion discussed in this subsection. This is based on the fact that as per the stoichiometric equation, the quantity of the CO<sub>2</sub> converted

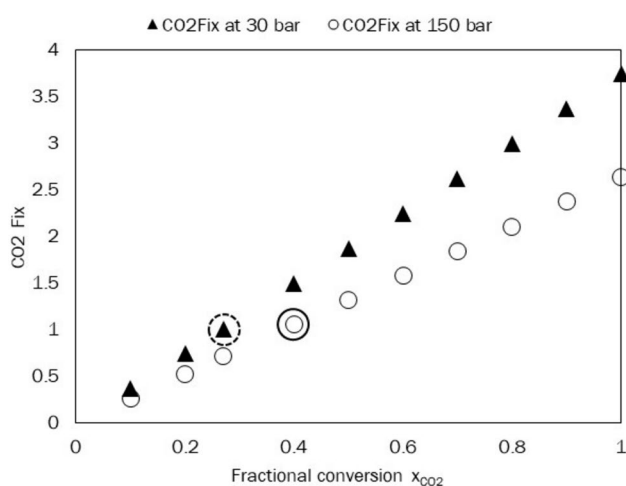


**Fig. 11** CO2Fix data for two pressure scenarios. At 30 bar, the conversion required to achieve a CO2Fix of 1 was 27%; at 150 bar, the required conversion was 40%

is equivalent to quantity of DMC produced.  $X_{CO_2}$  is the conversion of the subject reaction,  $\theta$  is a measure of CO<sub>2</sub> produced per unit of supplied energy [kg<sub>CO<sub>2</sub></sub>/kJ],  $Q$  is the energy required to heat the feed to the reaction temperature [kJ/kg feed], and  $W$  is the energy required to pressurize the feed to the reaction pressure [kJ/kg feed].

Additionally, when the feed materials are sourced from off-site locations, the compression and heating duties can be estimated as functions of the reaction pressure and temperature, respectively, using Eq. 10 and Eq. 11.

$$Q = 1.1272 \times T - 61.59 \quad (10)$$

$$W = 210.17 \ln(P) - 109.53 \quad (11)$$

where  $P$  is the pressure in bars and  $T$  is the temperature in °C.

As compression of fluids at high pressures can be energy intensive, running the reaction at higher pressures will lead to more CO<sub>2</sub> emissions than lower pressures. Utilizing the methodology developed by Ibrahim et al. [25] to estimate compression duty based on reaction pressure, the compression duties were estimated to be 944 kJ/kg and 713 kJ/kg for reactions conducted at 150 bar and 30 bar, respectively. Figure 11 depicts two pressure scenario comparisons for the CO<sub>2</sub>Fix potential of direct synthesis of DMC.

Using natural gas-based electricity as the power source and incorporating the specified heating and compression duties, the minimum requisite conversion for achieving CO<sub>2</sub> fixation (CO2Fix = 1) during operation at 150 bar was 40% (solid black circle in Fig. 11). When the reaction was operated at 30 bar, the minimum required conversion to reach CO<sub>2</sub> fixation was 27% (dotted black circle in Fig. 11).

However, both these required conversions are well outside the range of equilibrium conversions seen in Fig. 6. If the equilibrium is shifted through in-situ product removal, the conversions can be boosted to the values required for CO<sub>2</sub> fixation. The CO2Fix analysis of direct DMC synthesis using Eq. 9 indicates that the fixation potential is likely greater in low-pressure operations compared to high-pressure ones. However, it is important to conduct the CO2Fix analysis again under equilibrium-shifted conditions, as the dependency on pressure in a conversion occurring under such conditions may lead to improved fixation under high-pressure conditions.

## 5 Conclusions

This study presented a kinetic model for directly synthesizing DMC over nano-CeO<sub>2</sub> catalyst powder in low-pressure conditions. The observed low  $y_{DMC}$ , below 1%, align with previous research and emphasize the need for adjustments to the process to increase DMC production. This challenge arises from an “equilibrium lock” caused by simultaneous water production, which hinders the formation of DMC. Process modifications, such as reactive distillation or in-situ water removal using dehydrating agents, could shift the equilibrium towards increased DMC production, even when employing milder temperature and pressure conditions. The kinetics model introduced in this study helps predict outcomes under these different temperature and pressure conditions, which varies from previous studies focusing on high-pressure supercritical conditions. The developed kinetics model is specifically tailored for low-pressure, gas-phase conditions. Additionally, it performs reasonably well in liquid-phase scenarios with low liquid and high vapor proportions, but the most accurate predictions are provided in gas-phase conditions.

As only liquid samples were used in the experiments, the comparison was limited to the kinetics model’s predictions for the liquid phase. Notably, at a low temperature of 90 °C and a pressure of 30 bar, the kinetics model exhibited a significant deviation of –115% due to the high liquid-to-vapor ratio. This discrepancy decreased as the temperature increased and the system shifted more toward the vapor phase. Interestingly, at 120 °C, the difference between thermodynamics and kinetics predictions was less than 5%, showcasing the model’s precision in forecasting vapor-phase conditions. Moreover, when comparing the predictions from the kinetic model with the experimental data, a MAPE of 17% was evident, indicating a notable degree of predictability. Finally, the CO2Fix calculation demonstrates that, at a 27% conversion rate, the process can reach a net zero state at an operational pressure approximating 30 bar. Elevating the conversion rate



to higher levels yields a substantial increase in the CO<sub>2</sub>Fix metric, potentially reaching values in the vicinity of 3.5 or greater at conversion rates surpassing 95%.

**Acknowledgements** This work was made possible by NPRP, Qatar grant NPRP13S-0122-200141 from the Qatar National Research Fund (a member of the Qatar Foundation). The statements herein are solely the responsibility of the authors. Open Access funding provided by the Qatar National Library.

**Author Contributions** The authors' contributions to the paper are as follows: Hanif A. Choudhury contributed to the study's conceptualization, design, and draft manuscript. Gasim Ibrahim was key in data collection, kinetic model development, fitting, and the CO<sub>2</sub>Fix calculation. Mohamed Sufiyan Challiwalla was responsible for equilibrium assessment and Aspen calculations. Amara Abdelbar conducted the kinetic regime test and derived the kinetic models. Nimir O. Elbashir provided conceptualization, supervision, analysis, and interpretation of results and reviewed the draft. Kartick Mondal, Anuj Prakash, and Sabah Solim contributed to the interpretation of the kinetic model analysis and catalyst testing. All authors collectively reviewed the results and unanimously approved the final version of the manuscript.

**Funding** Open Access funding provided by the Qatar National Library.

**Data Availability** Not applicable.

## Declarations

**Competing interests** The authors declare that they have no known competing financial interests or personal relationships that could have appeared to influence the work reported in this paper.

**Open Access** This article is licensed under a Creative Commons Attribution 4.0 International License, which permits use, sharing, adaptation, distribution and reproduction in any medium or format, as long as you give appropriate credit to the original author(s) and the source, provide a link to the Creative Commons licence, and indicate if changes were made. The images or other third party material in this article are included in the article's Creative Commons licence, unless indicated otherwise in a credit line to the material. If material is not included in the article's Creative Commons licence and your intended use is not permitted by statutory regulation or exceeds the permitted use, you will need to obtain permission directly from the copyright holder. To view a copy of this licence, visit <http://creativecommons.org/licenses/by/4.0/>.

## References

- Santos BAV, Silva VMTM, Loureiro JM, Rodrigues AE (2014) Review for the direct synthesis of dimethyl carbonate. *ChemBioEng Rev* 1:214–229. <https://doi.org/10.1002/cben.201400020>
- Pacheco MA, Marshall CL (1997) Review of dimethyl carbonate (DMC) manufacture and its characteristics as a fuel additive. *Energy Fuels* 11:2–29. <https://doi.org/10.1021/ef9600974>
- Yoshida Y, Arai Y, Kado S et al (2006) Direct synthesis of organic carbonates from the reaction of CO<sub>2</sub> with methanol and ethanol over CeO<sub>2</sub> catalysts. *Catal Today* 115:95–101. <https://doi.org/10.1016/j.cattod.2006.02.027>
- Tomishige K, Ikeda Y, Sakaihoru T, Fujimoto K (2000) Catalytic properties and structure of zirconia catalysts for direct synthesis of dimethyl carbonate from methanol and carbon dioxide. *J Catal* 192:355–362. <https://doi.org/10.1006/jcat.2000.2854>
- Tomishige K, Sakaihoru T, Ikeda Y, Fujimoto K (1999) A novel method of direct synthesis of dimethyl carbonate from methanol and carbon dioxide catalyzed by zirconia. *Catal Letters* 58:225–229
- Lee HJ, Joe W, Song IK (2012) Direct synthesis of dimethyl carbonate from methanol and carbon dioxide over transition metal oxide / Ce Zr O catalysts : Effect of acidity and basicity of the catalysts. *Korean J Chem Eng* 29:317–322. <https://doi.org/10.1007/s11814-011-0185-3>
- Wu XL, Xiao M, Meng YZ, Lu YX (2005) Direct synthesis of dimethyl carbonate on H<sub>3</sub>PO<sub>4</sub> modified V<sub>2</sub>O<sub>5</sub>. *J Mol Catal A Chem* 238:158–162. <https://doi.org/10.1016/j.molcata.2005.05.018>
- Tamboli AH, Chaugule AA, Kim H (2017) Catalytic developments in the direct dimethyl carbonate synthesis from carbon dioxide and methanol. *Chem Eng J* 323:530–544. <https://doi.org/10.1016/j.cej.2017.04.112>
- Stoian D, Medina F, Urakawa A (2018) Improving the stability of CeO<sub>2</sub> catalyst by rare earth metal promotion and molecular insights in the dimethyl carbonate synthesis from CO<sub>2</sub> and methanol with 2-cyanopyridine. *ACS Catal* 8:3181–3193. <https://doi.org/10.1021/acscatal.7b04198>
- Bansode A, Urakawa A (2014) Continuous DMC synthesis from CO<sub>2</sub> and methanol over a CeO<sub>2</sub> catalyst in a fixed bed reactor in the presence of a dehydrating agent. *ACS Catal* 4:3877–3880. <https://doi.org/10.1021/cs501221q>
- Choi J, Han J (2016) Process development and economic analysis of carbon dioxide to dimethyl carbonate. In: 12th International Conference on Heat Transfer, Fluid Mechanics and Thermodynamics. Costa de Sol, pp 1232–1236
- Alexandratos SD (2009) Ion-exchange resins: a retrospective from industrial and engineering chemistry research. *Ind Eng Chem Res* 48:388–398. <https://doi.org/10.1021/ie801242v>
- Holtbruegge J, Heile S, Lutze P, Górák A (2013) Synthesis of dimethyl carbonate and propylene glycol in a pilot-scale reactive distillation column: experimental investigation, modeling and process analysis. *Chem Eng J* 234:448–463. <https://doi.org/10.1016/j.cej.2013.08.054>
- Pérez-Cisneros ES, Mena-Espino X, Rodríguez-López V et al (2016) An integrated reactive distillation process for biodiesel production. *Comput Chem Eng* 91:233–246
- Gomes VG, Lee S (2006) Reactive distillation. *Encycl Chem Process* 1:2541–2556
- Daful AG (2000) Simulation of reactive distillation: comparison of equilibrium and nonequilibrium stage models. *Int J Chem Mol Nucl Mater Metall Eng* 6:33–47. [https://doi.org/10.1016/S1385-8947\(99\)00114-X](https://doi.org/10.1016/S1385-8947(99)00114-X)
- Haßkerl D, Lindscheid C, Subramanian S et al (2018) Dynamic performance optimization of a pilot-scale reactive distillation process by economics optimizing control. *Ind Eng Chem Res* 57:12165–12181. <https://doi.org/10.1021/acs.iecr.8b01815>
- Hu X, Cheng H, Kang X et al (2018) Analysis of direct synthesis of dimethyl carbonate from methanol and CO<sub>2</sub> intensified by in-situ hydration-assisted reactive distillation with side reactor. *Chem Eng Process-Process Intensif* 129:109–117. <https://doi.org/10.1016/j.cep.2018.05.007>
- Wang F, Wei W, Su Y et al (2012) The design and simulation of the synthesis of dimethyl carbonate and the product separation process plant. *Distill - Adv from Model to Appl*. <https://doi.org/10.5772/38527>
- Huang Z, Li J, Wang L et al (2014) Novel procedure for the synthesis of dimethyl carbonate by reactive distillation. *Ind Eng Chem Res* 53:3321–3328. <https://doi.org/10.1021/ie403964q>
- Santos BAV, Pereira CSM, Silva VMTM et al (2013) Kinetic study for the direct synthesis of dimethyl carbonate from methanol and CO<sub>2</sub> over CeO<sub>2</sub> at high pressure conditions. *Appl Catal A Gen* 455:219–226. <https://doi.org/10.1016/j.apcata.2013.02.003>

22. Eta V, Mäki-Arvela P, Wärn J et al (2011) Kinetics of dimethyl carbonate synthesis from methanol and carbon dioxide over ZrO<sub>2</sub>-MgO catalyst in the presence of butylene oxide as additive. *Appl Catal A Gen* 404:39–46. <https://doi.org/10.1016/j.apcata.2011.07.004>
23. Marin CM, Li L, Bhalkikar A et al (2016) Kinetic and mechanistic investigations of the direct synthesis of dimethyl carbonate from carbon dioxide over ceria nanorod catalysts. *J Catal* 340:295–301. <https://doi.org/10.1016/j.jcat.2016.06.003>
24. Kabra SK, Turpeinen E, Keiski RL, Yadav GD (2016) Direct synthesis of dimethyl carbonate from methanol and carbon dioxide: a thermodynamic and experimental study. *J Supercrit Fluids* 117:98–107. <https://doi.org/10.1016/j.supflu.2016.05.039>
25. Ibrahim G, Challiwala MS, Choudhury HA et al (2023) CO<sub>2</sub>Fix: an approach to assess CO<sub>2</sub> fixation potential of CCU reaction pathways. *Comput Chem Eng*. <https://doi.org/10.1016/j.compchemeng.2023.108398>
26. Xuan K, Pu Y, Li F et al (2019) Metal-organic frameworks MOF-808-X as highly efficient catalysts for direct synthesis of dimethyl carbonate from CO<sub>2</sub> and methanol. *Chinese J Catal* 40:553–566. [https://doi.org/10.1016/S1872-2067\(19\)63291-2](https://doi.org/10.1016/S1872-2067(19)63291-2)
27. Jayakumar G, Irudayaraj AA, Raj AD (2017) Particle size effect on the properties of cerium oxide (CeO<sub>2</sub>) nanoparticles synthesized by hydrothermal method. *Mech Mater Sci Eng J* 9:2–7. <https://doi.org/10.2412/mmse.3.4.481>
28. Eta V, Leino AR, Mäki-Arvela P et al (2010) Synthesis of dimethyl carbonate from methanol and carbon dioxide: circumventing thermodynamic limitations. *Ind Eng Chem Res* 49:9609–9617. <https://doi.org/10.1021/ie1012147>
29. Atkins P, Jones L (2010) *Chemical principles; the quest for insight*, edition, F. W. H. Freeman and Company
30. De Buyl P, Varoquaux G, Gouillart E, et al (2020) *Scipy Lecture Notes*
31. Radhakrishnan K, Hindmarsh AC (1993) Description and use of LSODE, the livermore solver for ordinary differential equation, E-5843. *National Aeronautics and Space Administration Lewis Research Center Cleveland, Ohio*, pp 44135–53191
32. Camy S, Pic JS, Badens E, Condoret JS (2003) Fluid phase equilibria of the reacting mixture in the dimethyl carbonate synthesis from supercritical CO<sub>2</sub>. *J Supercrit Fluids* 25:19–32. [https://doi.org/10.1016/S0896-8446\(02\)00087-6](https://doi.org/10.1016/S0896-8446(02)00087-6)

**Publisher's Note** Springer Nature remains neutral with regard to jurisdictional claims in published maps and institutional affiliations.